ISSN 0016-7029, Geochemistry International, 2008, Vol. 46, No. 11, pp. 1145–1163. © Pleiades Publishing, Ltd., 2008.

SHORT COMMUNICATIONS

Geochemistry of Late Stage Medium to High-K Calc-Alkaline and Shoshonitic Dykes in the Ulukişla Basin (Central Anatolia, Turkey): Petrogenesis and Tectonic Setting[1]

M. A. Kurt[a], M. Alpaslan[a], M. C. Göncüoğlu[b], and A. Temel[c]

[a]*Mersin University, Department of Geology, 33343 Çiftlikköy/Mersin, Turkey*
[b]*Middle East Technical University Department of Geology, 06531 Anhara, Turkey*
[c]*Hacettepe University, Departent of geology, Anhara, Turkey*
e-mail: malikurt@mersm.edu.tr

Received May 23, 2007

DOI: 10.1134/S0016702908110062

INTRODUCTION

The Eurasian, African and Arabian plates meet in Turkey, and the Anatolian plate has evolved in response to subduction, collisions, and transcurrent motion among these plates. Anatolia contains fragments of oceanic and continental crust exposed in east–west trending tectonic belts (Fig. 1) that were formed during the closure of Tethyan Ocean in the Late Mesozoic and Early Cenozoic [1], [2]. The eastern Mediterranean region, including central Anatolia, experienced Alpine ophiolite emplacement, crustal thickening, magmatism and metamorphism during the end of Mesozoic, followed by the formation of several Tertiary basins (e.g. Sivas, Tuzgölü, Çankırı, etc., Fig. 1) above this convergent system [3]. Ulukışla Basin is one of these basins developed after the collision between Tauride–Anatolide and Pontide continental microplates during the Upper Cretaceous time. It had been recently considered as an example of a large extensional deep-water basin development above a suture belt [4].

The basin includes a very thick succession of deep-sea turbidites and pelagic carbonates associated with volcanic–volcanoclastic rocks of Upper Cretaceous–Middle Eocene age. By this it provides an opportunity to utilize igneous petrology for a better understanding of its geological evolution.

There are different interpretations on the geological evolution of the Ulukışla Basin. Initially, Görür et al. [3] assumed that it was formed as a forearc basin resulting from northward subduction of the Inner Tauride Ocean between the Bolkar Carbonate Platform to the south and Niğde-Kırşehir microcontinent to the north. In contrast, others advocated that the Ulukışla Basin occurred as a result of postcollisional extension [5], [6] or transtension [7] above the Tauride–Anatolide margin following the closure of the Neotethys. This was modified by Clark and Robertson [4] adopting the extensional (or transtensional) setting of the Ulukışla Basin but suggesting that is was developed on the suture zone of the Inner Tauride Ocean. Recently, detailed geochemical and isotope studies on the Late Cretaceous–Early Tertiary alkaline volcanic rocks of the Ulukışla Basin [8] and [9] were generated in relation to an extensional basin developed within the Tauride–Anatolide continental crust.

These early products of volcanic activity within the Ulukikışla Basin are intruded by a series of dioritic, monzogabbroic and trachytic dykes. They are mainly medium-high K calc-alkaline (diorite) and shoshonitic (monzogabbro and trachyte). It is known that within-plate potassic magmas are commonly generated during the extension and thinning of the lithosphere and upwelling of the asthenosphere [10]. They may display arc-type geochemical features, such as Colorado [11], Borneo [12], and Lachlan Fold Belt [13] or OIB-type features, such as Virunga Province [14].

In this paper, we will first discuss the genesis of these dykes, to find out the changes in the geochemistry of volcanic rocks in an evolving extensional system, and secondly we will try to understand the events that followed the initial extensional volcanism in Ulukışla area.

THEORETICAL BACKGROUND

The Ulukışla volcanosedimentary basin is bounded by the southern margin of the Central Anatolian Crystalline Complex [5] to the north, by the Bolkar Carbonate platform to the south and by the left-lateral Ecemiş fault zone and associated Oligo-Miocene deposits [15–17, 4] to the east (Fig. 1). It is the southern and central part of a complex basinal system that includes the

[1] The text was submitted by the authors in English.

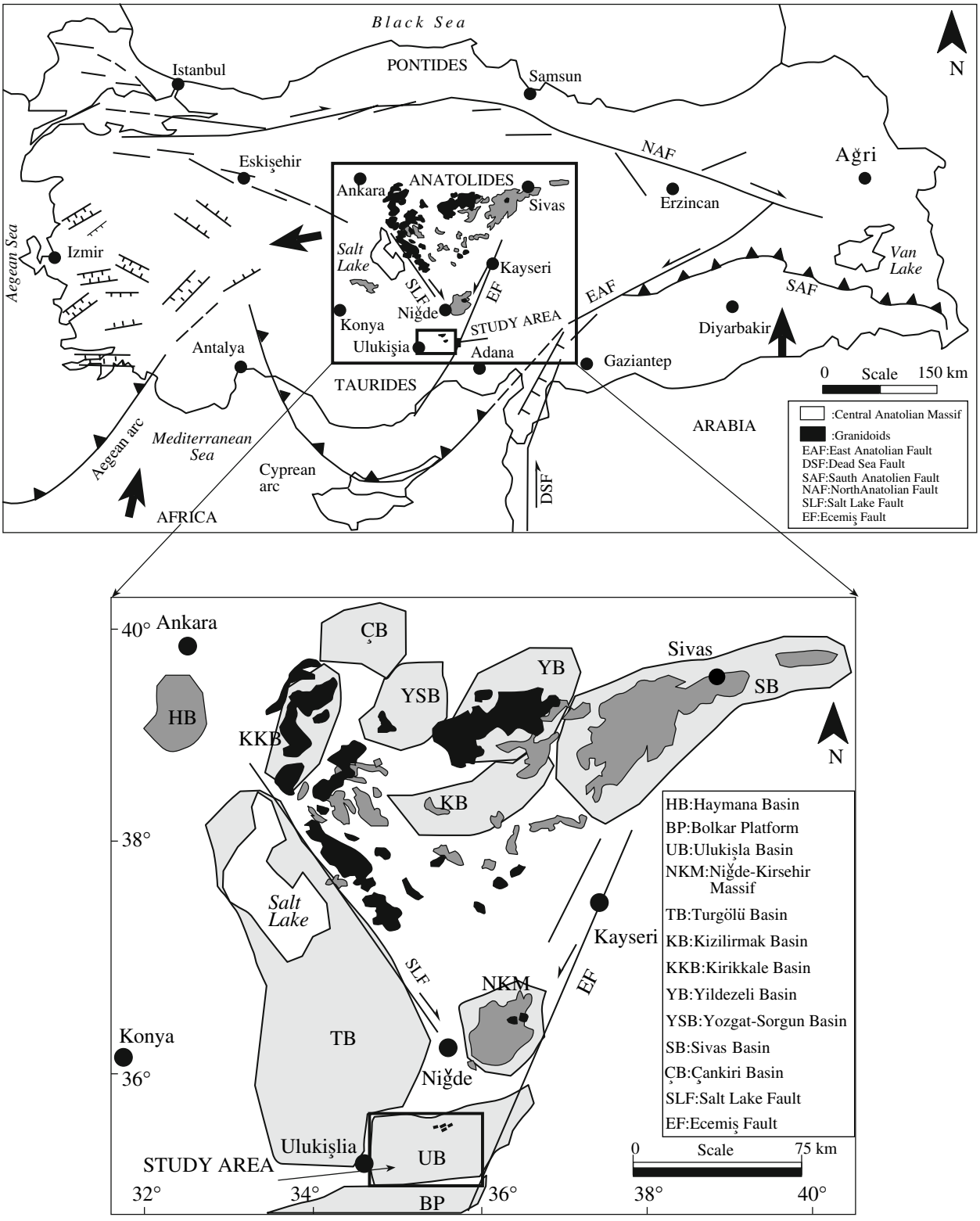

Fig. 1. Regional geological map and location of the study area (major sedimentary basins of central Anatolia. (BP, Bolkar Carbonate Platform; NKM, Nigde-Kirşehir Massif; UB, Ulukışla Basin, TB, Salt Lake Basin; HB, Haymana Basin; KKB, Kirikkale Basin; ÇB: Çankır Basin; YSB, Yozgat–Sorgun Basin; KB, Kizilirmak Basin; YB, Yildizeli Basin; SB, Sivas Basin; EF, Ecemiş Fault; SLF, Salt Lake Fault).

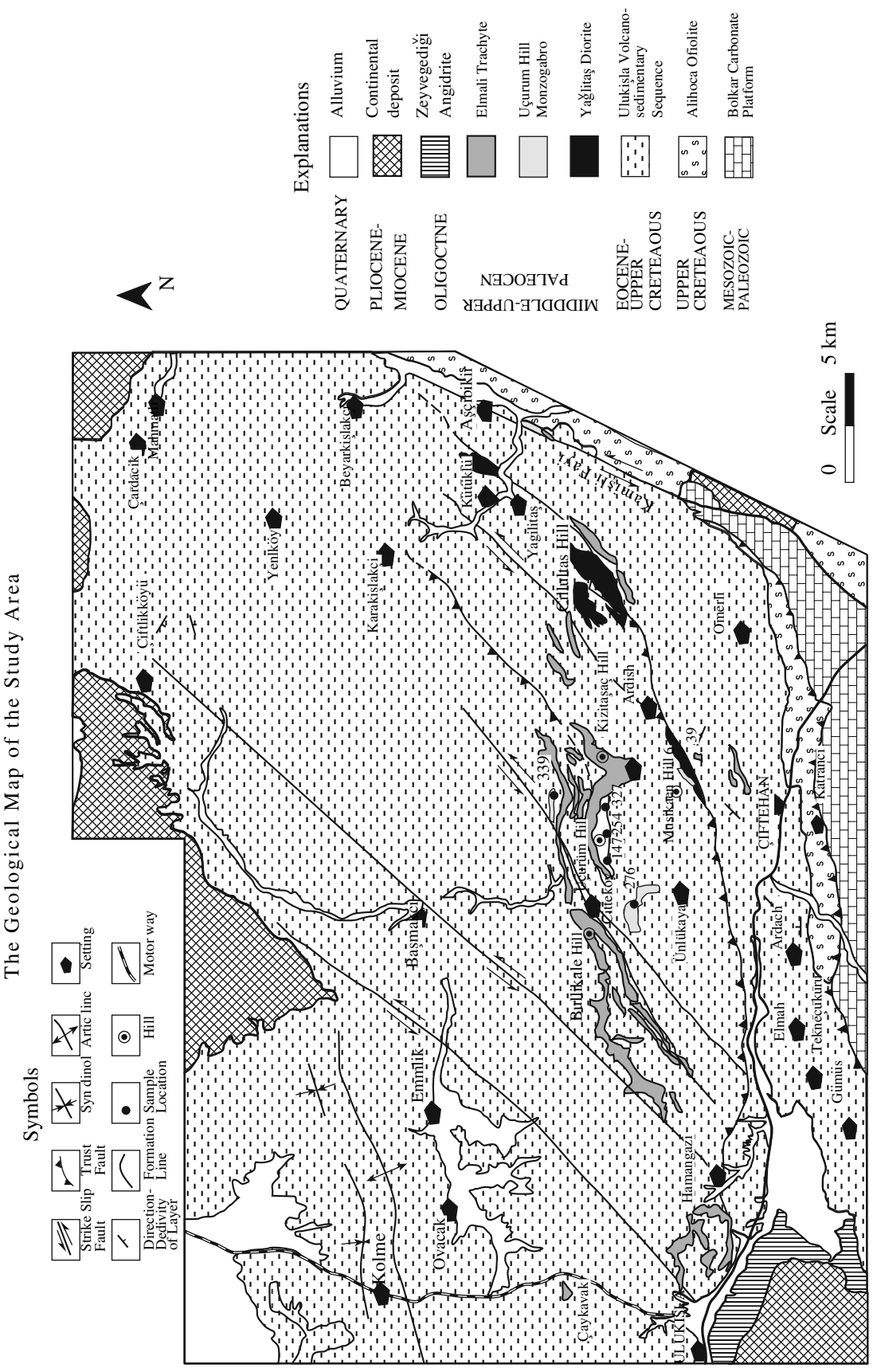

Fig. 2. Geological map of the study area (modified after [9]).

Tuzgölü Basin in NW and the Sivas Basin in NE [6]. The basin is floored by ophiolitic material (Alihoca Ophiolite), which was emplaced also onto the Bolkar Carbonate platform (Fig. 2), and contains Upper Cretaceous to Eocene volcanic and sedimentary sequences ([18], [19], [4], [9], Fig. 2). The thickness of the volcano-sedimentary sequences reaches up to several thousand meters [20], [21], [9]. The rock units in the Ulukışla Basin include flyschoidal sediments with patches and lenses of marl, pelagic limestone, reef limestone, claystone and volcanic rocks consisting of pillow and massive lavas and pyroclastic rocks [4], [8]. In the lower portion of the basin, pillow lavas occur at several stratigraphic horizons. Toward the middle part of the sequence, they gradually decrease in abundance and are replaced by massive lava flows at the top of the sequence [8]. The fossil findings from the associated sediments range from Late Cretaceous to Middle Eocene (Lutetian), indicating a continuous deposition, accompanied by volcanism.

The volcano-sedimentary rocks of the Ulukışla Basin are intruded by dioritic dykes trending in approximately ENE–WSW and monzogabbroic and trachytic dykes in the E–W direction (Fig. 2). Dioritic dykes outcrop in the Ulukışla volcanosedimentary sequence along a thrust zone in the NE–SW direction (Fig. 2). The thickness of the dioritic dykes varies from several ten centimeters to 250 m. They are crosscut by trachytic and ultrapotassic dykes. Monzogabbroic rocks occur as E–W tending dykes with varying thicknesses from a few meters to 150 meter within the volcanosedimentary sequence of the Ulukışla Basin (Fig. 2). Monzogabbros have also been crosscut by trachytic dykes. Their trend is E–W and they have a thickness between 1 to 200 m. Trachytic dykes were intruded by ultrapotassic dykes that were described by Alpaslan et al. [8]. They are the youngest representatives of the volcanic system and covered by sediments belonging to upper levels of the Ulukışla Basin and some ultrapotassic lavas.

METHODS

Forty-one fresh rock samples were selected for major, trace and rare earth element analyses (table). For major element analyses, fused disks were prepared using six parts of lithium tetraborate and one part rock powder. The mixtures were fused in crucibles of 95% Pt and 5% Au at 1050°C for 60 min to form a homogenous melt. The melt then was poured into a preheated mold and chilled as a thick glass disk. Whole rock analyses were performed at Hacettepe University using a PHILIPS PW 1400 X-ray spectrometer using USGS rock standards. Trace and rare earth element concentrations were analyzed at ACME laboratories (Vancouver, Canada) by ICP-MS using the fusion method; reported accuracy is better than ±3%.

EXPERIMENTAL RESULTS

1. Rock Types and Petrography

A total alkali-silica nomenclature diagram of Middlemost [22] shows that the monzogabbroic dykes mainly fall into the monzogabbro field above the dividing line between alkaline and subalkaline magmas, dioritic dykes into the gabbroic diorite field in the subalkaline field, and trachytes into the syenite field (Fig. 3A). Based on the normative mineral compositions, monzogabbros and most trachytes take place just on and below the dividing line between silica saturated and unsaturated magmas (Fig. 3B), whereas diorites fall into the diorite and quartz-monzodiorite fields (Fig. 3B). Monzogabbros and diorites are usually equigranular medium to coarse grained. Main mineral phases of the dioritic dykes are plagioclase, hornblende, biotite, and some quartz, whereas apatite, zircon, titanite and opaques are common accessories. In some diorites, clinopyroxenes have been observed as relicts surrounded by hornblende minerals. Hornblendes also occur as poiklitic minerals indicating the late-stage crystallization. In some diorites, hornblendes have been transformed into biotite. These biotites may be formed due to the reaction of K-bearing melt or hydrous melt with pre-existing hornblende or due to deuteric-hydrothermal alteration. Some plagioclases have sieve-textured zones indicating periods of dissolution and growth. Quartz generally occurs as anhedral minerals, which possibly indicate the crustal assimilation, between earlier formed minerals. Apatite commonly occurs in acicular character. Chlorite, epidote, and calcite occur as secondary minerals.

Mineral associations of the monzogabbro dykes are clinopyroxene, biotite, orthoclase, apatite, and opaque minerals. Clinopyroxene is often mantled by the biotite. Plagioclases can be divided into two categories based on textural criteria: (a) unsieved with no dissolution texture and (b) clear core mantled by a sieved zone and clear rim. Plagioclases include the clinopyroxene inclusions in sieved zones. Some biotites occur as poikilitic minerals implying late-stage crystallization. Apatite occurs as acicular, indicating the rapid growth in undercooled magma, [23] and prismatic forms. Chlorite, sericite, epidote, and calcite have been observed as secondary minerals.

Trachytes mainly have a hypocrystalline porphyrytic texture, but some samples have a holocrystalline porphyrytic texture. They contain sanidine, biotite, and a minor amount of clinopyroxene as phenocryst phases. Apatite occurs as microphenocryst in the groundmass. Groundmass includes the plagioclase microlithes, opaque minerals, and glass. Samdine phenocrysts have been transformed into clay minerals in some samples.

2. Major and Trace Elements

Major and trace element analyses of representative samples of the dykes are listed in the table. SiO_2 con-

Major, trace element analyses were given in weight % and ppm, of the selected rock samples (major and trace elements respectively; Fe_2O_3 as total Fe, LOI: loss on ignition)

Sample	D1	D2	D3	D4	D5	D6	D15	D17A
Longitude	34°46′18″	34°46′16″	34°46′14″	34°46′10″	34°46′12″	34°46′12″	34°46′11″	34°46′13″
Latitude	37°32′03″	37°32′04″	37°32′06″	37°32′05″	37°32′08″	37°32′08″	37°32′19″	37°32′23″
SiO_2	56.27	56.63	56.61	56.38	56.40	54.60	57.52	53.08
TiO_2	0.59	0.57	0.56	0.59	0.59	0.74	0.61	0.80
Al_2O_3	18.92	17.40	17.85	18.00	17.85	17.95	18.65	18.54
tFe_2O_3	6.84	7.14	6.48	6.64	7.15	7.57	4.41	8.02
MnO	0.13	0.12	0.13	0.13	0.14	0.14	0.06	0.15
MgO	3.27	4.20	2.97	3.30	3.27	4.14	3.32	4.34
CaO	4.44	3.92	5.70	5.67	4.41	6.63	4.83	7.44
Na_2O	4.20	5.01	4.49	4.17	4.39	4.02	6.22	4.22
K_2O	1.77	1.72	1.75	1.87	2.37	1.78	1.69	1.17
P_2O_5	0.22	0.20	0.19	0.20	0.20	0.16	0.14	0.19
LOI	3.44	2.49	2.48	2.50	2.62	1.64	1.63	1.73
Total	100.09	99.40	99.21	99.45	99.39	99.37	99.08	99.68
Rb	36.30	39.20	42.30	40.90	51.50	35.80	59.90	26.70
Cs	0.5	0.5	0.9	0.8	0.8	0.6	0.6	0.7
Ba	276.1	119.7	180.7	400.4	533.4	512.7	300.1	356.4
Sr	386.5	441.3	551.8	562.3	690.1	706.0	576.4	766.4
Ta	0.4	0.4	0.3	0.5	0.3	0.4	0.1	0.2
Nb	6.5	6.5	6.3	6.7	5.3	7.4	3.2	4.7
Hf	3.9	3.9	3.5	3.3	3.0	3.0	2.6	2.3
Zr	141.8	136.0	126.9	133.3	104.8	89.9	93.1	72.8
Y	20	21.3	19.5	19.3	18.8	22.3	19.5	21.3
Th	6.2	5.4	4.8	6.4	5.2	5.6	2.8	2.5
U	1.3	1.3	1.2	1.5	1.2	1.4	1.1	0.7
La	18.1	21.1	19.5	18.3	16.7	19.9	13.0	15.7
Ce	36.4	40.2	37.6	34.7	31.6	38.5	31.7	33.9
Pr	4.33	4.64	4.27	4.1	3.68	4.53	4.53	4.08
Nd	20.7	21.4	19.6	19.5	17.5	22.0	21.1	21.1
Sm	3.7	3.9	3.6	3.5	3.5	4.2	3.7	4.2
Eu	1.0	1.09	1.02	1.04	1.0	1.09	1.3	1.02
Gd	3.55	3.70	3.70	3.61	349	4.32	3.60	4.30
Tb	0.55	0.63	0.55	0.57	0.54	0.67	0.54	0.67
Dy	3.29	3.42	3.21	3.31	3.22	3.86	3.15	3.78
Ho	0.68	0.65	0.63	0.61	0.59	0.72	0.59	0.68
Er	1.84	1.98	1.78	1.95	1.85	1.96	1.78	2.01
Tm	0.28	0.28	0.29	0.28	0.27	0.28	0.27	0.27
Yb	2.07	2.01	2.03	1.97	1.68	1.86	1.70	2.06
Lu	0.34	0.35	0.31	0.33	0.32	0.32	0.30	0.31
Sample	D35	D36	D37A	D37B	D38	D39	D52	D53
Longitude	34°46′07″	34°46′08″	34°46′05″	34°46′05″	34°46′16″	34°46′15″	34°53′30″	34°53′35″
Latitude	37°32′20″	37°32′25″	37°32′21″	37°32′21″	37°32′17″	37°32′29″	37°35′51″	37°35′57″
SiO_2	53.52	55.09	56.63	56.74	56.37	55.07	48.85	48.89
TiO_2	0.78	0.50	0.55	0.64	0.54	0.61	1.15	1.23
Al_2O_3	18.40	18.26	17.76	17.77	17.69	18.47	19.08	18.78
tFe_2O_3	7.50	7.21	6.94	7.14	6.96	7.53	7.53	8.52
MnO	0.12	0.13	0.12	0.13	0.13	0.12	0.12	0.11
MgO	3.98	3.62	3.53	4.19	3.69	3.77	5.02	4.08
CaO	8.19	4.28	4.93	4.71	5.76	4.87	8.17	7.63
Na_2O	3.61	4.68	4.20	4.55	3.93	4.61	3.96	4.28
K_2O	1.24	2.17	2.14	2.31	1.59	1.69	2.58	2.35
P_2O_5	0.19	0.17	0.21	0.23	0.20	0.25	0.30	0.54
LOI	1.66	3.02	2.05	2.41	2.34	2.14	3.95	3.85
Total	99.19	99.13	99.06	100.82	99.20	99.13	100.71	100.26
Rb	25.8	44.7	46.3	40.8	33.6	55.2	67.0	87.5
Cs	0.9	1.0	1.1	1.1	1.1	1.6	2.6	4.5

Table. (Contd.)

Sample	D35	D36	D37A	D37B	D38	D39	D52	D53
Longitude	34°46′07″	34°46′08″	34°46′05″	34°46′05″	34°46′16″	34°46′15″	34°53′30″	34°53′35″
Latitude	37°32′20″	37°32′25″	37°32′21″	37°32′21″	37°32′17″	37°32′29″	37°35′51″	37°35′57″
Ba	389.9	483.3	443.8	536.2	364.0	925.0	675.0	719.7
Sr	801.7	539.5	574.9	542.4	613.2	754.5	798.4	712.2
Ta	0.4	0.4	0.4	0.4	0.4	0.4	0.5	0.5
Nb	5.0	4.8	5.2	4.7	5.0	5.3	8.7	9.6
Hf	3.4	3.5	4.1	2.7	3.1	2.7	2.9	3.6
Zr	109.9	104.4	140.9	99.2	102.8	83.5	121.4	142.2
Y	17.9	20.1	20.1	18.1	18.1	19.4	20.3	21.4
Th	5.1	5.3	5.9	4.4	3.9	7.5	9.5	13.3
U	1.1	1.2	1.6	1.2	0.9	1.4	2.3	3.1
La	20.2	14.7	15.8	13.3	14.7	13.1	39.6	63.8
Ce	41.3	31.5	35.4	30.0	31.8	32.4	76.9	122.1
Pr	4.83	3.81	4.26	3.52	3.67	4.02	7.61	12.19
Nd	21.2	17.7	20.0	17.3	18.2	19.5	31.6	48.5
Sm	4.0	3.5	3.6	3.5	3.2	3.9	5.8	8.3
Eu	1.14	0.94	1.02	0.89	0.96	1.15	1.69	2.23
Gd	3.84	3.67	4.05	3.30	3.56	4.15	4.61	5.67
Tb	0.6	0.6	0.58	0.54	0.59	0.62	0.66	0.72
Dy	3.37	3.42	3.52	3.02	3.14	3.4	3.45	3.74
Ho	0.55	0.64	0.65	0.6	0.56	0.64	0.62	0.62
Er	1.71	2.02	2.04	1.74	1.64	1.91	1.87	1.94
Tm	0.23	0.28	0.29	0.25	0.25	0.27	0.25	0.26
Yb	1.74	1.96	1.98	1.7	1.77	1.9	1.64	1.71
Lu	0.26	0.31	0.31	0.28	0.27	0.28	0.28	0.27
Sample	D354	D68	D71	D72	326	339	344	346
Longitude	34°53′40″	34°53′44″	34°53′49″	34°53′47″	34°45′10″	34°45′10″	34°46′20″	34°53′58″
Latitude	37°35′58″	37°36′01″	37°35′49″	37°35′49″	37°34′45″	37°34′25″	37°35′54″	37°35′57″
SiO_2	49.01	50.96	50.73	51.93	51.98	48.53	49.03	51.95
TiO_2	1.30	1.10	1.27	0.99	0.89	1.18	0.93	1.10
$Äl_2O_3$	19.76	18.17	18.37	18.44	19.86	20.33	21.44	18.33
tFe_2O_3	7.56	7.94	7.68	7.11	7.01	6.92	6.03	6.47
MnO	0.11	0.14	0.25	0.11	0.08	0.13	0.09	0.08
MgO	4.83	4.51	3.42	3.87	3.15	3.24	4.31	3.05
CaO	7.44	7.71	8.34	7.90	6.26	8.53	7.87	5.36
Na_2O	4.13	3.75	3.16	3.50	4.50	4.30	4.08	4.93
K_2O	2.40	2.66	2.86	3.06	3.41	1.66	2.21	3.05
P_2O_5	0.56	0.46	0.51	0.47	0.66	0.37	0.25	0.45
LOI	3.20	2.79	3.76	1.97	2.26	3.26	4.54	5.23
Total	100.30	100.19	100.35	99.35	100.06	98.45	100.78	100.00
Rb	80.2	68.6	99.9	97.7	104.3	50.4	67.7	83.9
Cs	2.8	2.1	2	2.1	2.6	2	2.3	2.1
Ba	1275.9	1711.8	1506.6	1606	1795.6	636	858.5	1572.7
Sr	877.6	903.7	726.6	796.9	1313.6	785.4	1097.5	759.1
Ta	J0.5	0.8	0.9	0.9	1.2	0.5	0.4	0.8
Nb	10	16	18	19	27.2	9.3	7.3	13.7
Hf	3.1	4.5	4.1	5.2	5.9	2.9	2.2	5.4
Zr	127.5	172.6	174.8	195.5	239.3	134.7	108.3	105
Y	22.1	24.9	25.6	25.7	26.8	22.9	17.4	26.5
Th	13.7	25.8	26.4	31.8	25.4	13	8.8	21.2
U	2.9	6.6	6.4	7.9	3.9	2.7	1.8	4.6
La	61.3	76.2	79.1	77.8	93.5	43.1	32.7	75.7
Ce	116.8	139.9	145.8	143.5	189.8	88	68.7	158
Pr	11.88	12.72	13.66	13.74	18.96	9.51	7.11	15.36
Nd	49.1	53.7	54.6	53.1	68.5	35.3	28.2	60.8
Sm	7.9	8.2	8.8	9.2	9.8	5.5	4.4	8.2

Table. (Contd.)

Sample	D354	D68	D71	D72	326	339	344	346
Longitude	34°53′40″	34°53′44″	34°53′49″	34°53′47″	34°45′10″	34°45′10″	34°46′20″	34°53′58″
Latitude	37°35′58″	37°36′01″	37°35′49″	37°35′49″	37°34′45″	37°34′25″	37°35′54″	37°35′57″
Eu	2.22	1.96	2.07	2.01	2.55	1.81	1.46	2.03
Gd	5.59	5.8	6.32	6.44	7.44	4.91	3.34	5.62
Tb	0.75	0.82	0.89	0.86	0.91	0.72	0.5	0.71
Dy	3.42	4.3	4.38	4.48	5.62	3.53	2.99	4.01
Ho	0.6	0.68	0.72	0.75	0.87	0.71	0.53	0.86
Er	1.86	2.09	2.31	2.4	2.18	1.93	1.49	2.02
Tm	0.28	0.29	0.26	0.31	0.34	0.29	0.21	0.31
Yb	1.65	1.92	1.88	2.21	2.18	1.89	1.42	2.13
Lu	0.28	0.28	0.29	0.26	0.32	0.26	0.27	0.31
Sample	D62	D63	257	260	261	264	325	327
Longitude	34°53′40″	34°53′39″	34°37′15″	34°37′20″	34°37′23″	34°37′28″	34°45′16″	34°45′17″
Latitude	37°36′07″	37°36′02″	37°44′49″	37°44′45″	37°44′43″	37°44′42″	37°34′41″	37°34′35″
SiO_2	46.86	48.05	49.01	48.16	48.61	49.72	47.16	49.34
TiO_2	1.46	1.36	1.11	1.04	0.94	1.13	1.13	1.45
Al_2O_3	17.24	18.50	20.02	19.67	20.72	19.76	19.72	18.95
tFe_2O_3	8.27	7.07	7.25	7.83	6.99	7.27	7.37	8.46
MnO	0.14	0.14	0.15	0.09	0.09	0.08	0.14	0.17
MgO	5.54	6.49	3.76	3.07	3.65	4.01	5.38	3.91
CaO	9.72	8.67	6.05	8.79	9.07	7.20	9.20	6.17
Na_2O	3.33	3.19	4.52	2.82	2.91	3.37	2.87	3.52
K_2O	2.99	2.76	3.33	3.22	3.56	3.96	3.00	4.18
P_2O_5	0.45	0.24	0.70	0.75	0.63	0.69	0.75	0.74
LOI	3.54	3.63	4.22	3.14	2.52	2.38	3.66	2.47
Total	99.54	100.10	100.12	98.58	99.69	99.57	100.38	99.36
Rb	37.2	27.2	173.90	120.90	114.4	140.5	109.9	189.4
Cs	1.1	1.5	4.20	1.20	1.20	1.40	2.40	4.80
Ba	533.6	435.4	1597.6	1785.9	1774.7	1835.4	1796.5	3189.6
Sr	773.8	929.2	1268.8	1272.0	1316.8	1171.8	1264.6	1370.2
Ta	0.4	0.4	1.00	1.20	1.00	1.20	0.9	1.40
Nb	8	7.3	29.8	26.3	21.3	29.3	21.9	33
Hf	3	3.2	7.3	5.5	5.1	6.5	4.6	8
Zr	116.6	115.6	281.40	242.5	188.4	257.4	190.2	333.5
Y	23.2	20.7	34.1	29.6	25.9	29.7	26.4	35.5
Th	10.4	8	28.1	20.4	21.2	25.5	17.3	31.8
U	2.1	2.1	4.2	4.2	3.5	3.9	3	5.5
La	41	35.8	114.6	99.9	83.1	91	70.8	114.7
Ce	81.6	68.3	250.8	214.6	171.7	189	155.4	267.2
Pr	8.67	7.04	25.35	20.85	17.73	19.53	16.08	26.57
Nd	35.4	30	93	81.1	69.8	73.1	61.9	102.4
Sm	6.7	5.4	15.8	12.5	10	11.1	9.9	15
Eu	1.87	1.76	3.28	2.74	3.03	2.91	2.58	3.48
Gd	5.19	4.53	8.61	7.93	7.61	7.77	7.19	10.47
Tb	0.77	0.67	1.33	1.01	0.89	0.95	0.92	1.28
Dy	3.99	3.55	6.09	5.16	5.41	6.01	4.8	6.56
Ho	0.67	0.59	1.03	0.9	0.85	0.89	0.89	1.11
Er	2.11	1.88	2.69	2.66	2.5	2.59	2.11	2.81
Tm	0.28	0.25	0.42	0.36	0.35	0.34	0.3	0.42
Yb	1.76	1.54	2.52	2.02	2.24	2.4	2.18	2.46
Lu	0.29	0.25	0.37	0.37	0.43	046	0.33	0.46

Table. (Contd.)

Sample	2	10	73	86	236	285	295	334
Longitude	34°32′55″	34°32′09″	34°41′59″	34°42′29″	34°44′18″	34°47′05″	34°46′56″	34°45′04″
Latitude	37°32′10″	37°33′20″	37°35′41″	37°35′15″	37°36′32″	37°34′11″	37°34′05″	37°33′49″
SiO_2	63.35	60.2	60.31	59.23	59.34	63.77	63.23	63.69
TiO_2	0.36	0.54	0.47	0.51	0.6	0.35	0.56	0.44
Al_2O_3	18.28	17.47	18.29	18.49	18.02	17.76	17.52	1696
tFe_2O_3	3.43	3.39	3.97	4.16	4.14	2.48	3.45	3.42
MnO	0.07	0.12	0.07	0.12	0.06	0.03	0.04	0.05
MgO	0.24	1.03	1.60	1.74	1.70	0.44	1.68	0.35
CaO	0.66	1.38	0.87	0.86	0.73	0.21	0.50	0.31
Na_2O	6.46	3.80	3.50	2.07	2.41	3.27	4.80	5.40
K_2O	5.97	8.85	9.03	10.78	10.41	9.25	4.82	5.62
P_2O_5	0.08	0.09	0.21	0.15	0.15	0.06	0.20	0.14
LOI	0.94	1.69	1.54	1.60	1.66	1.42	2.11	1.23
Total	99.84	98.56	99.86	99.71	99.22	99.04	98.91	97.61
Rb	161.1	247.2	157.2	364.3	201.8	297.8	149.8	176.5
Cs	0.4	3.3	1.1	1.2	1.0	1.9	2.8	1.4
Ba	1339.6	544.8	1665.6	1296.3	4025.4	1196.6	1625.6	2077.8
Sr	257.9	382.1	347.2	663.5	361	100.2	262.3	188.4
Ta	2.1	1.7	1.6	1.4	1.3	2.3	1.3	1.3
Nb	37.9	40.1	38.3	34.5	30.7	48.3	17.9	20.3
Hf	12.5	9.8	9.8	9	8.2	10.3	8.1	8.2
Zr	500.5	430.3	410.7	386.7	343	445.6	314.4	331.6
Y	31.4	40.8	34.7	40	36	37.6	17.4	28
Th	60.4	54.6	53.5	52.1	37.7	79.7	58.1	42.3
U	6.8	5.2	8.1	7.7	6.3	10.9	10.3	7.6
La	92.9	139.5	150.9	129.5	105.5	211.4	64	105.5
Ce	177.6	270.9	297	258.8	211.8	405.8	108.1	199.8
Pr	17.49	28.09	30.65	27.65	22.2	39.56	12.31	19.6
Nd	59	99	107.6	101.4	79.7	134.7	41.4	64.2
Sm	8.7	14.7	14.8	15.3	11.9	17.9	5.3	8.3
Eu	1.74	3.13	3.23	3.81	3.06	2.44	0.97	1.98
Gd	6.05	9.41	8.02	9.99	7.78	9.3	2.79	4.81
Tb	1.03	1.41	1.27	1.45	1.22	1.48	0.46	0.82
Dy	5.13	6.94	5.93	6.52	5.94	6.7	2.47	4.43
Ho	1.05	1.25	1.02	1.21	1.16	1.18	0.56	0.93
Er	2.95	3.37	2.89	3.25	3.13	3.53	1.84	2.78
Tm	0.47	0.49	0.46	0.48	0.45	0.54	0.34	0.47
Yb	3.32	3.43	2.9	3.06	3.01	3.79	2.4	3.02
Lu	0.5	0.51	0.43	0.47	0.45	0.56	0.41	0.47

tents range from 53.14 to 56.74% in the diorites, whereas it ranges from 46.86 to 51.95% in the monzogabbros and from 59.23 to 63.77% in the tyrachytes. The data are illustrated in a total alkali-silica diagram in Fig. 5a. The diorites fall into the subalkaline field, whereas monzogabbros and trachytes fall into the alkaline field (Fig. 3A). When all samples are plotted on the SiO_2-K_2O diagram of Peccerillo and Taylor [24], diorites show middle to high K character, and monzogabbros and trachytes indicate a shoshonitic character (Fig. 4A) according to the criteria defined by Morrison [25], with $K_2O + Na_2O > 5\%$, high K_2O/Na_2O ratios (>0.6 at $SiO_2 = 50\%$, >1.0 at $SiO_2 = 55\%$), low TiO_2 (generally <1.3%), and high but variable $A1_2O_3$ (14%–19%). Diagrams based on trace element data also reveal that the diorites have calcalkaline, and monzogabbros and trachytes have shoshonitic character (Fig. 4B). Major elements against SiO_2 variations indicate that the Fe_2O_3t, TiO_2, MgO, CaO, and P_2O_5 decrease with increasing SiO_2, whereas Na_2O increases (Fig. 5), although P_2O_5 content of the diorites is nearly constant (Fig. 5). Incompatible trace elements such as Rb, La, Th, U, Nd, Nb, Y, and Yb indicate positive correlations against Zr (Fig. 6), but Ba and Sr have variable and scattered values (table). Primitive mantle normalized trace element patterns (Fig. 7) summarize the distinctive features shared by both calk-alkaline and shoshonitic dykes. All dykes show significant enrichments in large-ion lithophile elements (LILE) relative to high field strength elements (HFSE) and HREE accompanied by distinct negative anomalies for Nb–Ta and Ti (Fig. 4A). A positive Sr and negative Ba anomalies in calk-alkaline diorites and negative Sr anomaliy in the shoshonitic monzogabbros and trachytes occur (Fig. 7).

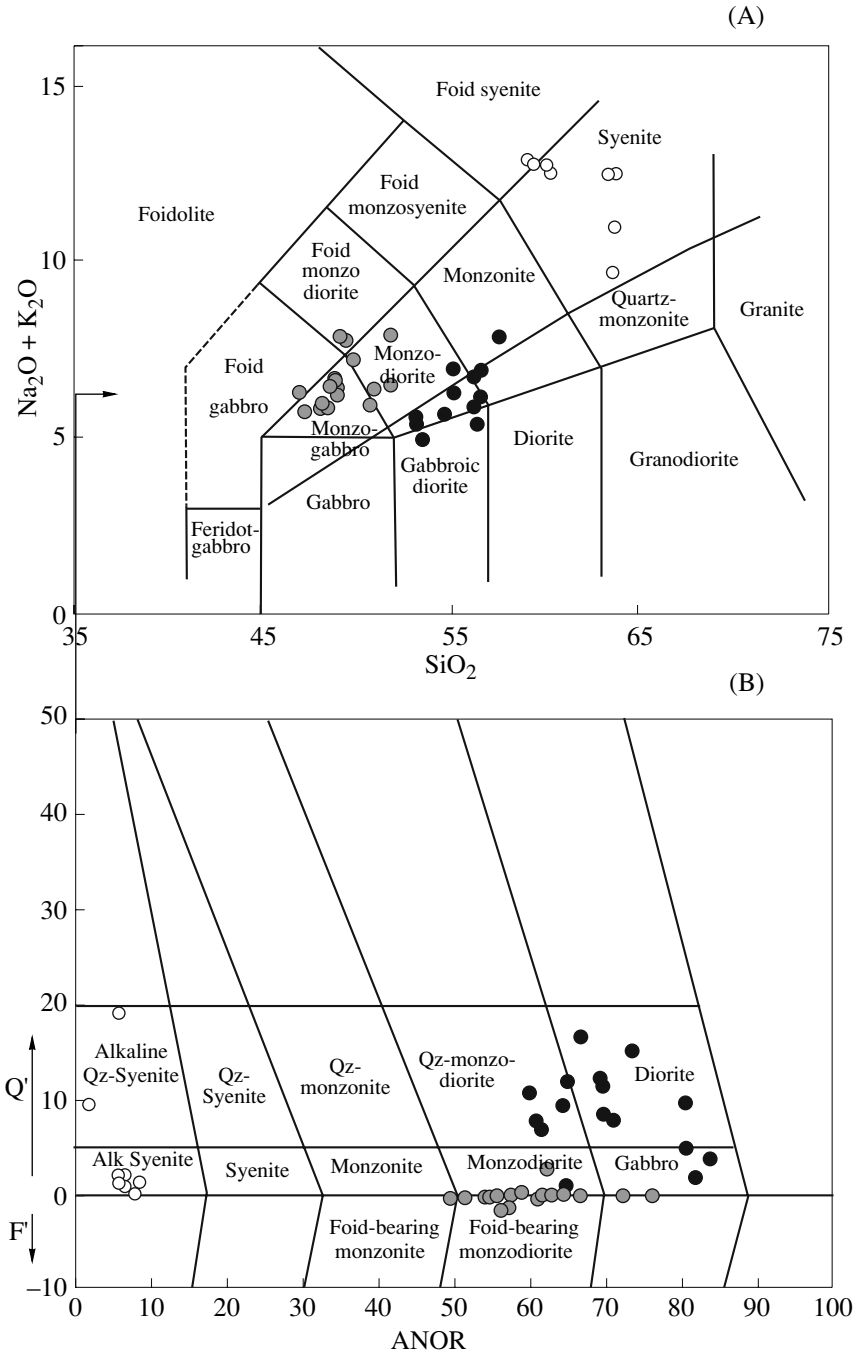

Fig. 3. Geochemical classification of the dykes. (A) Total-alkali versus silica nomenclature diagram [54] for the dykes, line distinguishing between alkalic and subalkalic rocks after Irvine and Baragar [55]; (B) Q'F'—ANOR diagram [56] using normative compositions, Q' = Q/(Q + Or + Ab + An) 100, F' = (Ne + Lc + Kp)/(Ne + Lc + Kp + Or + Ab + An) 100, ANOR = An/(Or + An) 100 (Symbols; ◍ LU Monzogabbro, ● Diorite, ○ Syenite).

Trace element patterns of all dykes in Fig. 7 are similar to those of subduction-related mafic rocks, which have been significantly contaminated or derived from a lithospheric mantle, modified by earlier subduction process [26–28]. In Fig. 7, monzogabbros and trachytes also show small depletions in Zr and Hf. These depletions relative to LILE and LREE enrichment have been originated from subduction related material, which is present in the mantle source region [27]. All dykes are considerably enriched in LREE relative to primitive mantle, resulting La_N/Yb_N ratios that range from 5.49–8.33 for diorites, 16.36–35.48 for monzogabbros, and 19.13–40.02 for trachytes. All dykes have similar patterns, which tend to be flattened out in the LREE, and

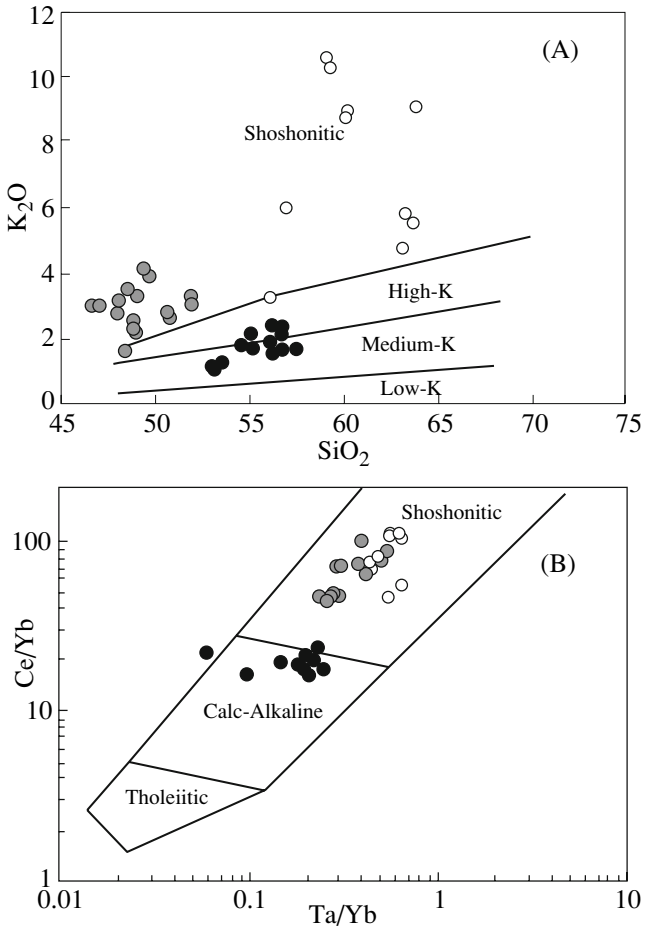

Fig. 4. (A) K_2O-SiO_2 [24] and (B) Th/Yb–Ce/Yb [57] diagrams showing magma character for studied dykes (symbols as in Fig. 3).

flatten in the HREE (Fig. 8). Monzogabbros and trachytes are more enriched in LREE than diorites. Small negative Eu anomalies in the diorites are indicative of fractional crystallization involving plagioclase (Fig. 8). La/Sm and Sm/Yb ratios point to the presence of garnet as a residual phase during the generation of the shoshonitic dykes, whereas those ratios exclude the presence of residual garnet for generation of the calk-alkaline dykes (Fig. 9).

DISCUSSION

For both calc-alkaline and shoshonitic dyke suites, a general fractional crystallization trend is suggested by decreasing MgO, Fe_2O_3total, CaO, TiO_2, and P_2O_5 and increasing Na_2O (Fig. 5); shoshonitic ones having a compositional gap at 52 to 59% SiO_2. Trace element variations also indicate trends suggesting fractionation for both suites, but they are different in their incompatible trace element contents (table and Fig. 6). The variation of these elements are due to fractionation of clinopyroxene, amphibole, titanite, titanomagnetite, and apatite, whereas the high concentrations of Ba and K_2O contents of the shoshonitic dykes may point to K-feldspar accumulation in the crystallization history. Both associations show patterns that indicate enrichment in LILE and LREE relative to primitive mantle (Figs. 7 and 9). "To account for these enrichments, which is accompanied by depletion of Nb and Ta relative to LILE and LREE, two different mechanisms have been invoiced for these rocks: (1) crustal contamination of mantle-derived melt and (2) derivation from an enriched mantle source.

1. The Compositional Gap

A compositional gap subdivides the shoshonitic dykes into a bimodal rock series, namely monzogabbro and trachyte. Such compositional gaps have been described by various researchers [29–35]. McBirney et al. [31] proposed that such compositional gaps may occur due to sidewall crystallization, compositional convection, and collection of evolved liquid at the top of a magma body (i.e., liquid fractionation). Groove and Donnely–Noan [32] also proposed that SiO_2 gaps develop as a result of small temperature decreases in the magma chamber, resulting in a high degree of crystallization and increased viscosity. The interruption of magma replenishment entails closed system behavior of the magma chamber with continuing crystallization [36]. The viscosity of the magma body increased to a critical level, suppressing magma rising due to the increase of SiO_2 polymerisation. Subsequently, the enrichment of incompatible elements (especially H_2O) in the residual melt leads to SiO_2 depolymerization and thus to a decrease in viscosity, whereby the magma becomes able to erupt, but with more felsic composition [36].

Monzogabbros have been characterized by the presence of two plagioclase generations with and without reaction rims indicative for a longer storage time. In addition, unhydrous mineral phases such as clinopyroxene are mantled by hydrous phases (such a biotite). However, no trachyte samples contain monzogabbroic xenoliths, which is an indication that a different process was responsible.

According to Fig. 10, a distinction into two rock groups is also evident on the basis of REE data. Generally, REE data exhibit parallel patterns (Fig. 10). Trachytes are more enriched in LREE relative to HREE. Slight enrichments in REE for monzogabbros can be explained by increasing amount of clinopyroxenes during magma evolution. In contrast, REE patterns of trachytes reveal steep negative slopes for the LREE relative to D63, which is a more primitive sample of the monzogabbroic suite (Fig. 10). All trachyte samples yield more negative Eu/Eu* values than those of monzogabbros (Fig. 10). Thus, the compositional gap mentioned above also appears in trace element composition.

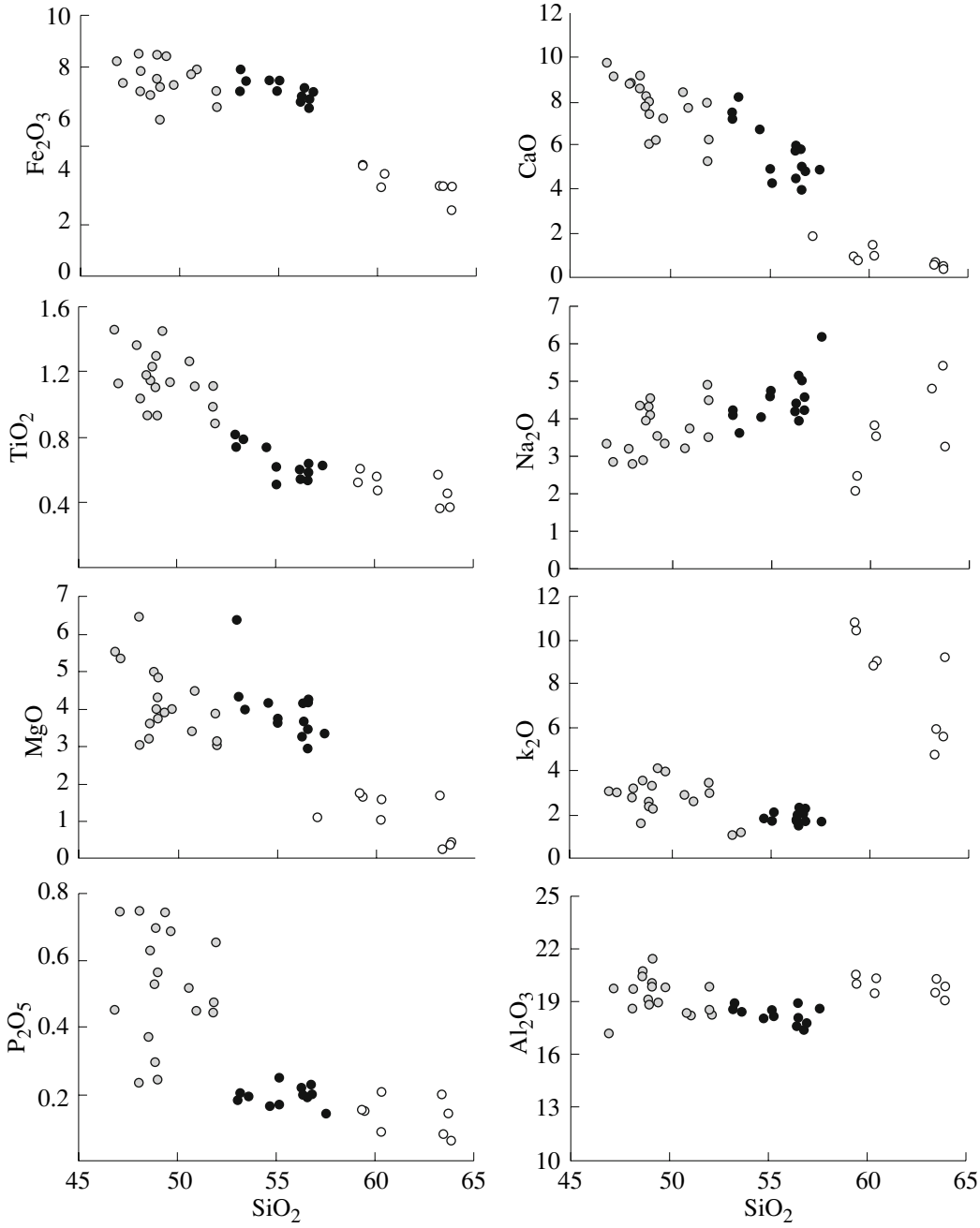

Fig. 5. Major element variations against SiO_2 for dykes (symbols as in Fig. 3).

2. Crustal Contamination

The fact that the magma was ascended through continental crust raises the possibility that crustal contamination may have produced some of the compositional characteristics of the studied volcanic rocks. Indeed, diorites and monzogabbros exhibit features that can be attributed to such a process. Crustal assimilation may produce some trace element variations observed in Figs. 5 and 6. However, it does not explain the very high concentrations of Sr (max values: diorites—801 and monzogabbros—1268 ppm) and Ba (max. values: diorites—925; monzogabbros—3189; and trachytes—4025) (table), which are much higher than the continental crustal values (Ba—390 ppm; Sr—325 ppm, [37]). They have low Nb/La (e.g., diorites—0.24–0.40; monzogabbros—0.15–0.32; and trachytes—0.19–0.41 vs. mantle—1.0) and high Th/La (diorites—0.15–0.57 and monzogabbros—0.20–0.40 vs. mantle ~0.12; [38]) ratios. Ratios of incompatible trace elements, such as Rb/Nb and Zr/Nb (not shown), increase with increasing SiO_2 suggesting crustal contamination during the evolution of the diorites (e.g., [39]), while, in the

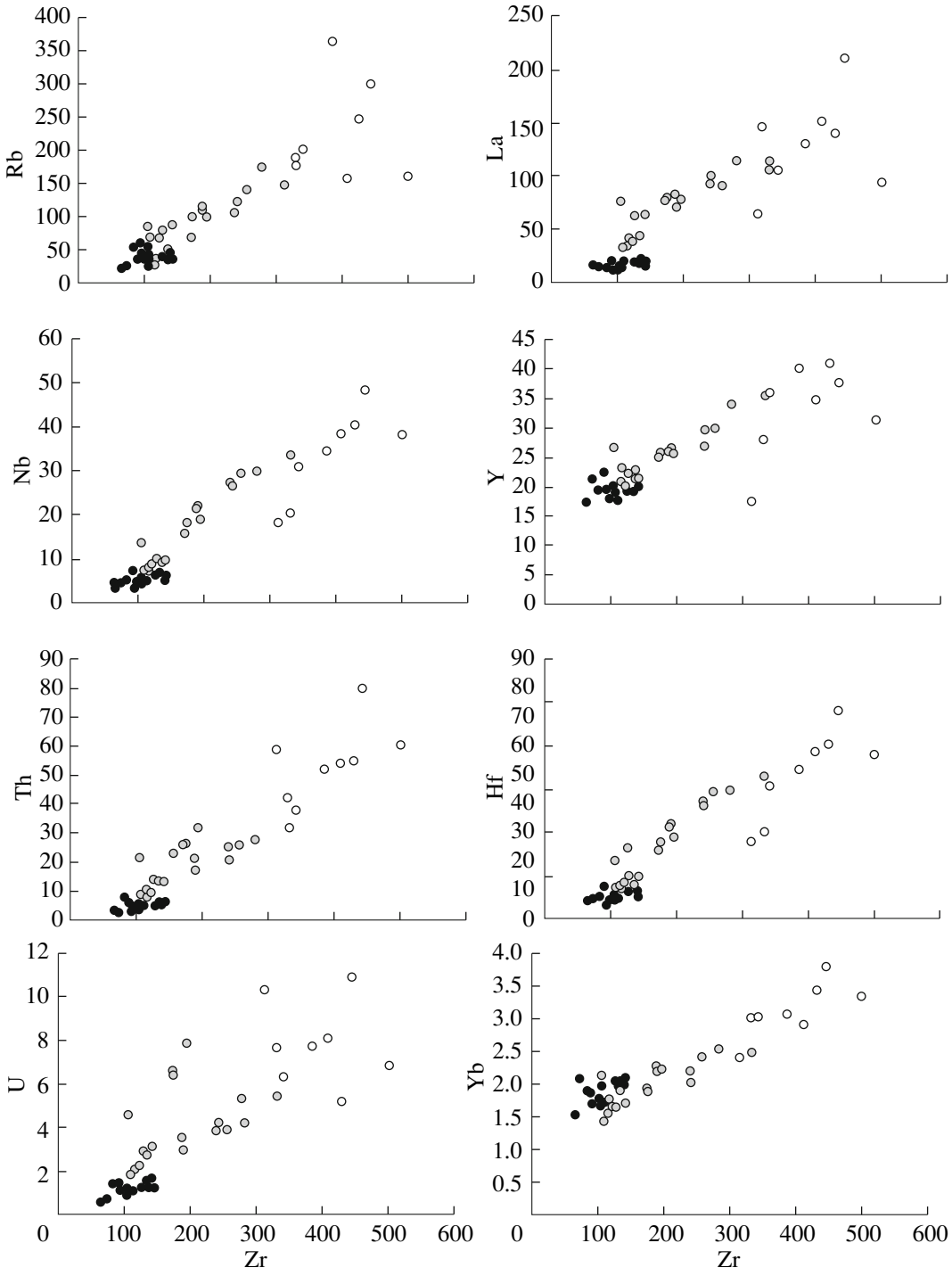

Fig. 6. Trace element vs. Zr variation diagrams for dykes (symbols as in Fig. 3).

monzogabbros and trachytes, Rb/Nb ratios vary in a large range, but Zr/Nb, in a narrow range (table). Assimilation of continental crust is inconsistent, not only with the high LILE and LREE contents, but also with relatively low Rb/Sr and Rb/Ba ratios. These data combined with primitive mantle-normalized trace element and REE patterns exclude crustal assimilation to have played a significant role in the pedogenesis of the shoshonitic dykes, although variations of these ratios in the calk-alkaline dykes indicate signs of the crustal assimilation of the magma. Crustal assimilation can also be found in the petrographical features of some

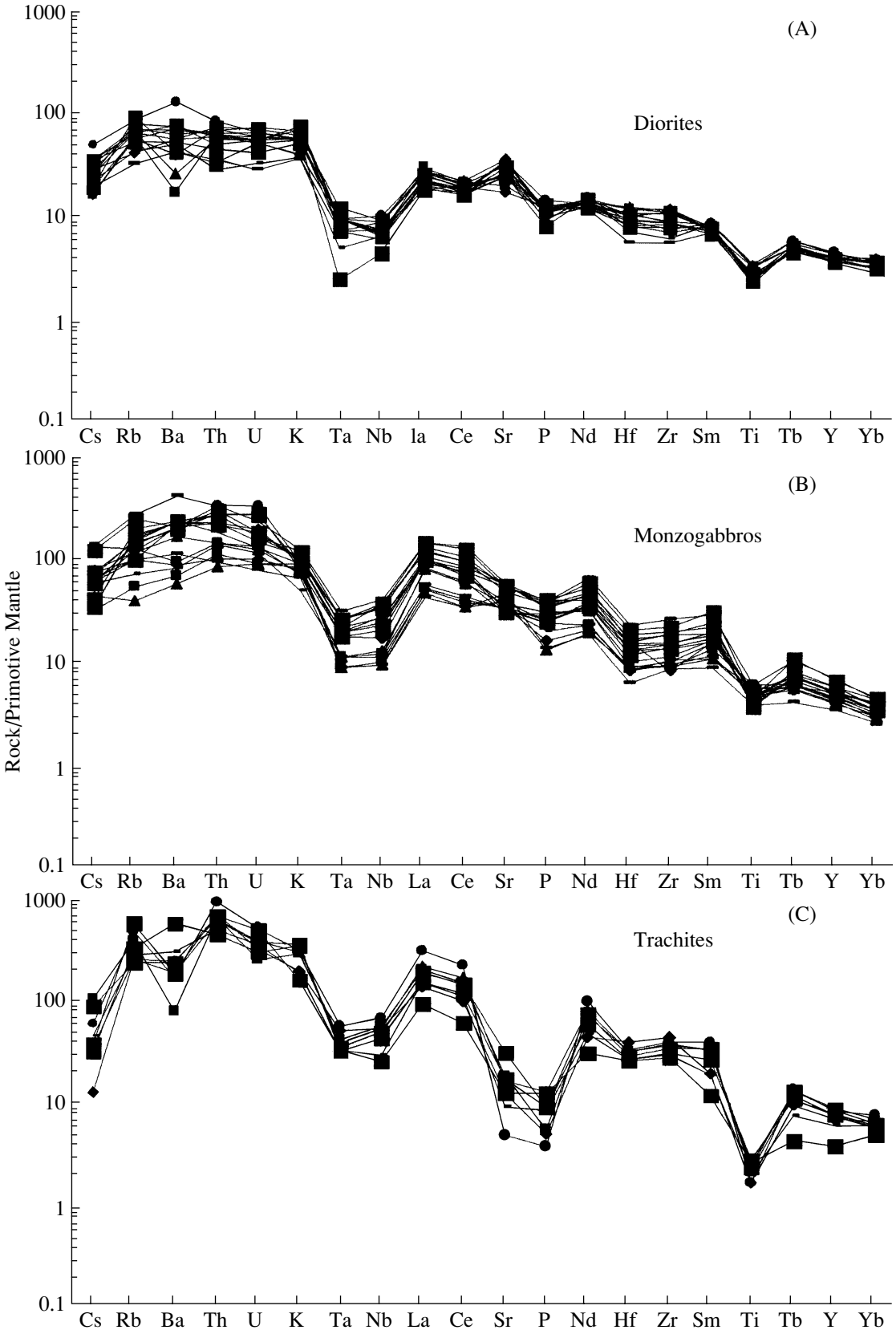

Fig. 7. Primitive mantle-normalized trace element patterns for dykes: (A) diorites, (B) monzogabbros, and (C) trachytes (normalized values from [38]).

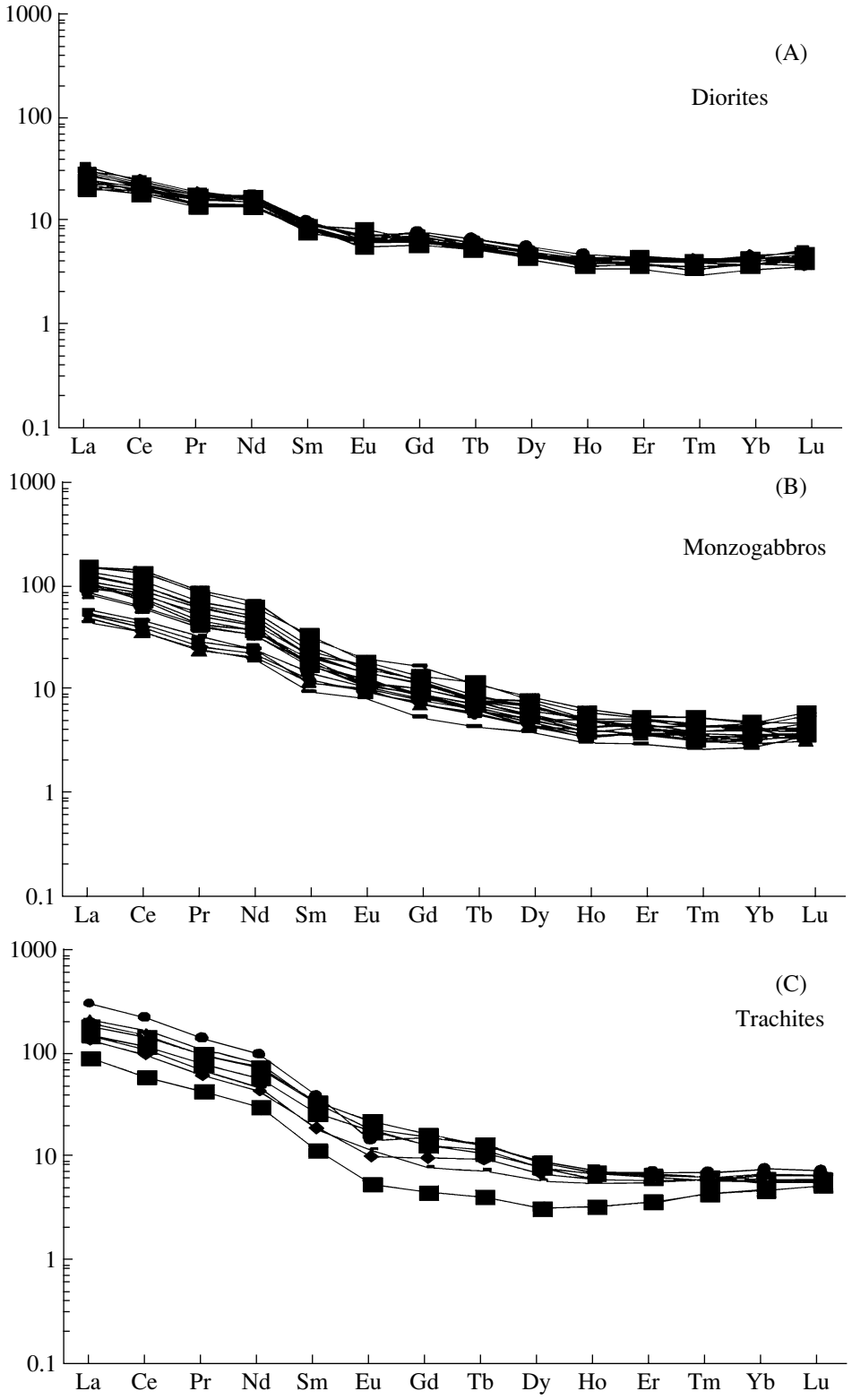

Fig. 8. Primitive mantle-normalized REE patterns for dykes: (A) diorites, (B) monzogabbros, and (C) trachytes (normalized values from [38]).

diorites that contain some quartz and zircon. Thus, it can be concluded that the crustal assimilation process may play a role on the evolution of the calc-alkaline diorites but have a smaller or no effect on the evolution of the shoshonitic monzogabbros and trachytes.

3. Source Heterogeneity

Both of calk-alkaline and shoshonitic dykes demonstrate higher La/Nb (diorites—2.47–4.04; monzogabbros—3.10–6.64; trachytes—3.37–5.19), Ba/Nb (diorites—28.68–174.52; monzogabbros—53.61–117.60; trachytes—13.58–103.35), Th/La (diorites—0.19–0.57; monzogabbros—0.20–0.40; trachytes—0.35–0.90), Th/Ta (diorites—9.75–18.75; monzogabbros—17–35.33; trachytes—29–44.69), lower Nb/La, Ba/La (diorites—5.67–31 with exception sample D39; monzogabbros—11.28–27.80; trachytes—5.66–38.15), and Nb/U (diorites—3.25–6.71; monzogabbros—2.81–7.51; trachytes—1.73–7.71) ratios in comparison with those of OIB [38]. Such signatures are distinct from those of asthenosphere-derived magmas characterized by the enrichment of LILE, LREE, and HFSE with Nb/La ratio >1. These rocks also have incompatible trace element patterns, which are different from those of asthenosphere-derived magmas (Fig. 7). High Ba/Nb and La/Nb ratios, which are higher than those of island arc volcanics and crustal values, and positive anomalies for Ba, Th, and U for shoshonitic dykes require source enrichments in these elements and point to different degrees of involvement of a subduction component in the genesis of the shoshonitic magmas. In addition, active subduction as a source for these magmas is, however, highly improbable in view of the postcollisional nature of these rocks. This shape of the primitive mantle-normalized trace element patterns may reflect subduction-related processes that modified the lithospheric mantle. Ba, Th, and U values that are higher than those of island arc magmatism and crustal values require source enrichments and point to different degrees of subduction component involvement in the genesis of the both calc-alkaline and shoshonitic dykes. These ratios require a distinct mantle source and exclude magmas produced by any model involving partial melting of the MORB and OIB.

In regard to the HFSE anomalies of the calk-alkaline and shoshonitic dykes in the Ulukışla Basin, their extremely high LILE/HFSE ratios clearly suggest that these two groups of elements were fractionated with respect to each other at some stage of the magma generation or during metasomatism. This fractionation could have been produced by the presence of HFSE-bearing phase in residium [40], [41]. This hypothesis agrees with the narrow range of the HFSE contents of the calk-alkaline and shoshonitic dykes (table). This relationship could be easily generated by variable degrees of partial melting with HFSE buffered at low values by residual titanites. Alternatively, the high

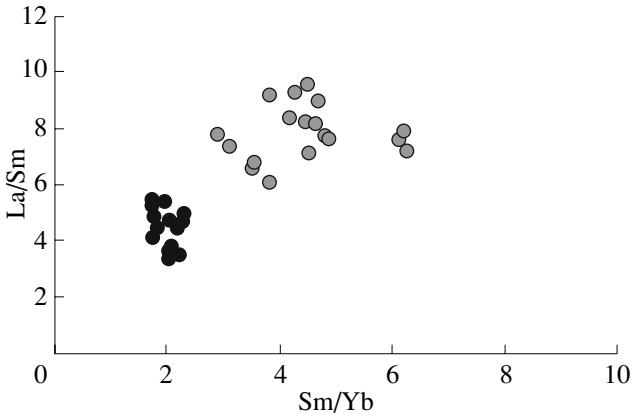

Fig. 9. La/Sm vs. Sm/Yb diagram for dykes (symbols as in Fig. 3).

LILE/HFSE values may result from addition to the sources of different amounts of melts or fluids already depleted in HFS elements, which generated a variable enrichment in LIL elements, leaving HFSE at their original concentrations. Ancient subduction events might have caused a large scale recycling of the subducted slab. During these events, incompatible element-rich fluids and sediments may have entered into the lithospheric mantle, causing enrichments in LILE. The addition of LILE via a fluid to mantle peridotite is consistent with the relatively high solubility of these elements in hydrous fluids [42]. The addition of HFSE via a fluid phase is generally considered unlikely due to low solubility of these elements in hydrous fluids [43]. Low Nb/U ratio and high La/Nb and Ba/Nb ratios may have been resulted from metasomatism due to a fluid-dominated process. On the other hand, superchondritic Zr/Hf ratios of the monzogabbros and trachytes together with their relatively higher P contents indicate that enrichment was caused by mantle metasomatism assisted by CO_2 rich fluids (e.g. [44]). The contributions of Th and U, which are less mobile than the other large

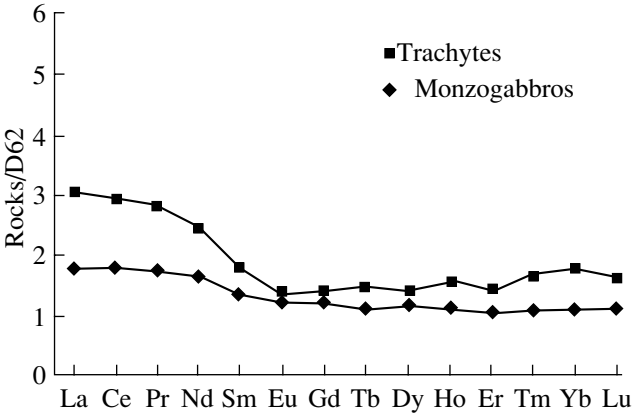

Fig. 10. Rare earth element distributions of the monzogabbros and trachytes relative to D-63.

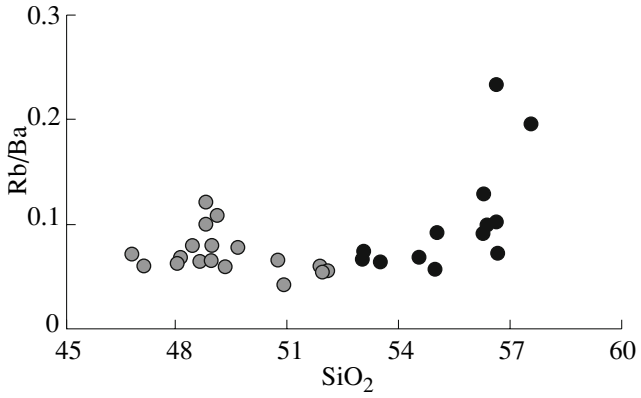

Fig. 11. Rb/Ba vs. SiO_2 diagram for dykes (symbol as in Fig. 3).

ion lithophile elements, are more controversial. Their characteristics suggest a low mobilization in the fluid component. The presence of Th in subduction related magmas is generally explained by melting of pelagic sediments (e.g., [45]). This indicates that this element is derived from sediments and tends to be transferred over a long time period compared with fluids [46], [47]. Th and U enrichments relative to LILE (Fig. 9) require a contribution of sediments from the subducted slab during earlier subduction events, possibly closure of the southern branch of the Neotethys. Results depicted above for the evolution of the study area suggest the presence of a heterogeneously metasomatized subcontinental–lithospheric mantle (possibly sort of leopard-skin mantle) during the Tertiary, which was able to produce a wide range of magmas ranging from calc-alkaline to shoshonitic.

The potassic nature of the studied dykes requires that a K-rich mineral, such as phlogopite, was present in the upper mantle and melted to produce the ultrapotassic magmas. The variable potassium contents probably reflect melting of different amounts of phlogopite. However, phlogopite is not a typical mantle mineral and its presence in the upper mantle reveals compositional anomalies [48]. A phlogopite-bearing lithospheric mantle, metasomatized by subduction-related fluids or melts as discussed above, may be suggested as the source of these magmas [41], [49]. Small-scale heterogeneity is commonly considered to be due to the presence of a vein network permeating the upper-mantle peridotite [50]; the veins are inferred to be rich in clinopyroxene together with accessory phases, such as phlogopite, titanite, and oxides, uncommon in normal peridotitic mantle assemblages. The range of variation in the trace element (LREE/HFSE) characteristics and isotopic characteristics of both associations might to be attributed to small-scale mantle heterogeneity. In particular, variation in the trace element ratios (LREE/HFSE) might be attributed to variable roles in the residuum for accessory phases (e.g., phlogopite and apatite) or the difference in the relative proportion of veins and peridotitic wall-rock components, which contribute to the melt. The partition coefficients for LREE in apatite dominate those of LREE in the other mineral phases in the veins (e.g., clinopyroxene); thus, apatite controls the LREE characteristics [51]. The presence of apatite in the residuum of partial melting of the veins could produce the negative anomaly (Fig. 7). Calk-alkaline diorites and shoshonitic monzogabbros have negative P anomalies, suggesting that apatite was stable and not completely melted out from the vein component in the mantle source.

The Rb/Ba vs. SiO_2 diagram show lower and similar ratios of Rb/Ba for monzogabbros and diorites (Fig. 11; trachtyes are not included in this diagram because of their highly evolved nature). This ratio increases with increasing SiO_2 in the diorites, which is related to fractionation. Ba is partitioned into phlogopite to a greater extent than Rb [51]; thus, partial melts, which have phlogopite in the residium, will acquire a high Rb/Ba ratio, whereas significant removal of phlogopite from the residium by partial melting of the veins will tend to decrease the Rb/Ba ratios. Lower Rb/Ba ratios of the both group might be related to significant melting of phlogopite from the source.

La/Sm vs. Sm/Yb diagram (Fig. 9) for calk-alkaline and shoshonitic dykes indicates that both groups of dykes cannot be originated by the partial melting of the same source material. It also reveals that the calk-alkaline dykes were originated from a garnet-free source, possibly the spinel–peridotite field, and shoshonitic dykes originated from a garnet-bearing source. As a whole, geochemical characteristics of the calk-alkaline and shoshonitic dykes strongly suggest the presence of the heterogeneously metasomatized lithospheric mantle, able to produce the calc-alkaline and shoshonitic magmas.

4. Tectonic Implications

Volcanism represented by the alkaline series in the Ulukışla Basin has been proposed as being formed in an intracontinental extensional setting [8] and [9] in association with the development of the basin [4] and [9] during Late Cretaceous to Early Tertiary. Such intracontinental volcanisms marked by subduction-related geochemical fingerprints are not unusual in orogens (e.g., [52], [53]). Recent studies on volcanic rocks within the Ulukışla Basin suggest that these magmas have been originated from an enriched subcontinental lithospheric mantle source based on geochemical and isotope data and occurred in an extensional tectonic setting [8], [9]. The closure of the Ulukışla basin was achieved by compressional tectonic regime toward the end of Lutetian by east–west trending and south–vergent thrust faults and imbrications [8].

Both calc-alkaline and shoshonitic dykes intruding alkaline volcanics and intercalated sedimentary units of the Ulukışla Basin are approximately oriented in east–

west (Fig. 2). Calc-alkaline diorites occur just within the main thrust zone, which is capable of transporting melt from mantle. Therefore development of the calc-alkaline diorites is possibly related to the compressional tectonic phase in response to the closure of the Ulukışla Basin. Their enriched nature and metasomatized mantle origin, indicated by enrichment of incompatible trace elements and depletion in high-field strength elements may imply that the subcontinental lithospheric mantle still persists during the closure of the basin. However, some petrographical and geochemical characteristics of the diorites imply the presence of crustal assimilation processes during the evolution of these rocks.

In brief, the geochemical data together with field observations indicate that the extensional tectonic phase in Late Cretaceous was followed by compressional tectonics related to the closure of the Ulukışla Basin in the Lutetian time. During these events, faulting of the crust, sufficient to generate fractures capable of tapping the base of the lithospheric mantle, leads to emplacement of shoshonitic dykes, which derived from melts occurred by partial melting of more enriched mantle domain beneath central Anatolia.

CONCLUSIONS

The volcanism in the Ulukışla Basin in central Anatolia is represented by an earlier phase (Late Cretaceous) of alkaline rocks, formed by postcollisional extension [8], [9]. It is followed by E–W trending dykes of two distinct magmatic suites: calk-alkaline diorites and shoshonitic monzogabbros and trachytes. Geological and major and trace element compositions of these two suites indicate the following features:

(1) Calk-alkaline diorites emplaced within the ENE–WSW trending thrust zone intrude the volcanosedimentary sequence of the Ulukışla Basin. They are crosscut by E–W trending dykes of shoshonitic monzogabbros and trachytes.

(2) Fractional crystallization process may be responsible for geochemical variations within individual suites. The shoshonitic suite has a compositional gap.

(3) Both suites share the marked enrichments in LILE and LREE and depletions in HFSE (i.e., Nb, Ta and Ti). Shoshonitic dykes are more enriched in LILE and present more steeply fractionated REE patterns than the calk-alkaline diorites.

(4) Primitive mantle-normalized trace and REE patterns; higher La/Nb, Ba/Nb, and Th/La ratios; and lower Nb/La, Ba/La, and Nb/U ratios of both suites indicate that they were originated from a mantle source enriched by subduction-related fluids or melts. These data suggests that the metasomatized mantle, previously enriched during the subduction processes, resulted from convergence between Eurasia and Arabia–Africa plates and still persists under the central Anatolia during Tertiary.

(5) Geochemical characteristics of both suites and geological relationships represent that the emplacements of the calk-alkaline and shoshonitic dykes are possibly related with compressional tectonics due to the Middle Eocene closure of the extensional Ulukışla Basin.

ACKNOWLEDGMENTS

This study was mainly funded by Mersin University Research Fund, under the project of BAP-FBE-JM (MAK)2003-1YL, and partly by Scientific and Technical Research Council of Turkey (TUBITAK), under the Project of YDABÇAG 100Y010. The authors are grateful for their economic support.

REFERENCES

1. A. M. C. Sengör and Y. Yilmaz, "Tethyan evolution of Turkey: a Plate Tectonic Approach," Tectonophysics **75**, 181–241 (1981).
2. A. H. F. Robertson, J. E. Dixon, Introduction: Aspects of the Geological Evolution of the Eastern Medterranean; in *Geol. Evol. East. Mediterranean*, 1–74 (1984).
3. N. Görür, O. Tüysüz, and A. M. C. Sengör, "Tectonic Evolution of the Central Anatolian Basins," Int. Geol. Rev., No. (1998), 831–850.
4. M. Clark and A. Robertson, "The Role of the Early Tertiary Ulukisla Basin, Southern Turkey in Suturing of the Mesozoic Tethys Ocean," J. Geol. Soc. London, **159**, 673–690 (2002).
5. M. C. Göncüoğlu, G. M. V. Toprak, G. M. V. Kuşçu, et al., "Geology of the Western Part of the Central Anatolian Massif, Part 1: Southern Part," (METU-TPAO Project Report, Ankara, 1991).
6. I. Cemen, M. C. Göncüoglu, and K. Dirik, "Structural Evolution of the Tuzgölü Basin in Central Anatolia, Turkey," J. Geol. **107**, 693–706 (1999).
7. K. Dirik, M. C. Göncüoğlu, and H. Kozlu, "Stratigraphy and Pre-Miocene Tectonic Evolution of the Southwestern Part of the Sivas basin, Central Anatolia, Turkey," Geol. J. **34**, 303–319 (1999).
8. M. Alpaslan, D. Boztuğ, A. Ucurum, and Z. Özdemir, "Petrology of the Çamardı-Ulukışla Paleocene–Eocene Volcanics and Gold Potential of the Hydrothermal Occurences," TUBITAK Project, YDABÇAG, Y010 (2003).
9. M. Alpaslan, R. Frei, D. Boztuğ, et al., "Geochemical and Pb–Sr–Nd Isotopic Constraints for an Enriched-Mantle Source for the Late Cretaceous to Early Tertiary Volcanism in the Çamardı-Ulukışla Basin, Niğde Province, Central Anatolia, Turkey,". Int. Geol. Rev. **46**, 1022–1041 (2004).
10. D. Müller and D. I. Groves, *Potassic Igneous Rocks and Associated Gold-Copper Mineralization,* (Springer, New York, 2000).
11. P. T. Leat, R. N. Thompson, M. A. Morrison, et al., "Compositionally diverse Miocene-Recent rift related

magmatism in northwest Colorado: Partial melting and mixing of mafic magmas from, 3 Different Asthenosphere and Lithospheric Mantle Sources," J. Petrol. Spec. Lithos. Issue, 251–377 (1988).

12. S. C. Bergman, D.P. Dunn, and L. G. Krol, "Rock and Mineral Chemistry of the Linhaisai Minette, Central Kalimantan, Indonesia, and the Origin of Borneo Diamonds," Can. Mineral. **26** (1), 23–43 (1988).
13. D. Whyborn, "The Tectonic Significance of Ordovician Magmatism in the eastern Lachlan Fold Belt," Tectonophysics **214**, 177–192 (1992).
14. N. W. Rogers, D. James, S. P. Kelley, and M. Demulder, "The Generation of Potassic Lavas from the Eastern Virunga Province, Rawanda," J. Petrol. **39**, 223–247 (1998).
15. C. Yetiş, "New Observations on the Age of the Ecemiş Fault," in *Proceedings of International Symposium on Geology of the Taurus Belt,Ankara, Turkey, 1984* Ed. by O. Tekeli and M. C. ve Göncüoğlu (Ankara, 1984).
16. A. Koçyiğit and A. Beyhan, "A New Intracontinental Transcurrent Structure: The central Anatolian Fault Zone, Turkey," Tectonophysics **284**, 317–337 (1998).
17. N. Jaffey and A. H. F. Robertson, "New Sedimentological and Structural Data from Ecemis. Fault Zone: Implications for Timing and Offset and the Cenozoic Tectonic Escape of Anatolia," J. Geol. Soc. London **158**, 367–378 (2001).
18. J. M. L. Cater and J. R. Gillcrist, "Karstic Reservoirs of the Mid-Cretaceous Mardin Group, SE Turkey: Tectonic and Eustatic Controls on the Genesis, Distribution and Preservation," J. Petrol. Geol. **17**(3), 253–278 (1994).
19. C. Yetiş, G. Kelling, S. L. Gökçen, and F. Baroz, "A Revised Stratigraphic Framework for Later Cenozoic Sequences in the Northeastern Mediterranean Region," Geol. Rundsch. **84**, 794–812 (1995).
20. F. Y. Oktay, "Ulukışla ve *Cevresinin Stratigrafisi ve Jeolojik Evrimi,*" Türkiye Jeol. Kur. Bült. **25**, 1–24 (1982).
21. A. Çevikbaş, and Ulukışla-Çamardı (Niğde), "Tersiyer Havzasmm Jeodinamik Evrimi ve Maden Yataklan Yonunden Onemi," Doktora tezi l. Ü. Müh. Fak. Jeoloji Müh. Bölümü, 235 s. (yayimlanmamiş), (Istanbul, 1991).
22. E. A. K. Middlemost, "Naming Materials in the Magma/Igneous Rock System," Earth-Sci. Rev. **37**, 215–224 (1994).
23. M. J. Hibbard, *Petrography to Pedogenesis,* (Prentice Hall, New Jersey, 1995).
24. A. Peccerillo and S. R. Taylor, "Geochemistry of Eocene Calc-Alkaline Volcanic Rocks from Kastamonu Area, Northern Turkey," Contrib. Mineral. Petrol. **58**, 63–81(1976).
25. G. W. Morrison, "Characteristics and Tectonic Setting of the Shoshonite Rock Association," Lithos. **13**, 97–108 (1980).
26. C. J. Hawkesworth and R. Vollmer, "Crustal Contamination vs. Enriched Mantle $^{143}Nd/^{144}Nd$ and $^{87}Sr/^{86}Sr$ Evidence from the Italian Volcanics," Contrib. Mineral. Petrol. **69**, 151–165 (1979).
27. P. D. Kempton, J. G. Fitton, C. J. Hawkesworth, and D. S. Ormerod, "Isotopic and Trace Element Constraints on the Composition and Evolution of the Lithosphere beneath the Southern United States," J. Geophys. Res. **96**, 13713–13735 (1991).
28. J. Dostal, B. L. Cousens, and C. Dupuy, "The Incompatible Element Characteristics of an Ancient Subducted Sedimentary Component in Ocean Island Basalt from French Polyniesia," J. Petrol. **39**, 937–952 (1998).
29. R. N. Thompson, "Evidence for a Chemical Discontinuity near the Basalt–Andesite Transition in Many Anorogenic Colcanic Suites," Nature **236**, 106–110 (1972).
30. B. H. Baker, G. G. Goles, W. P. Leeman, and M. M. Linstrom, "Geochemistry and Petrogenesis of a Basalt–Benmoreite-Trachyte Suite from the Southern Part of the Gregory Rift, Kenya," Contrib. Mineral. Petrol. **64**, 303–332 (1977).
31. A. R. McBirney, B. H. Baker, and R. H. Nilson, "Liquid Fractionation. Part I. Basic Principles and Experimental Simulations," J Volcanol. Geotherm. Res. **24**, 1–24 (1985).
32. T. L. Grove and J. M. Donnelly-Nolan, "The Evolution of Young Silicic Lavas at Medicine Lake Volcano, California: Implications for the Origin of Compositional Gaps in Calc-Alkaline Series Lavas," Contrib. Mineral. Petrol. **92**, 281–302 (1986).
33. B. D. Marsh, "Solidification Fronts and Magmatic Evolution," Mineral Mag. **60**, 5–40 (1995).
34. G. M. Thompson, I. E. M. Smith, and J. G. Malpas, "Origin of Oceanic Phonolites by Crystal Fractionation and the Problem of the Daly Gap: an Example from Rarotonga," Contrib. Mineral. Petrol. **142**, 336–346 (2001).
35. A. Peccerillo, M. R. Barberio, G. Yirgu, et al., "Relationships between Mafic and Peralkaline Silicic Magmatism in Continental Rift Settings: a Petrological, Geochemical and Isotopic Study of the Gedemsa Volcano, Central Ethiopian Rift," J. Petrol. **44** (11), 2003–2032 (2003).
36. A. Buettner, I. C. Kleinhanns, D. Rufer, et al., "Magma Generation at the Easternmost Section of the Hellenic Arc: Hf, Nd, Pb and Sr Isotope Geochemistry of Nisyros and Yali Volcanoes (Greece)," Lithos. **83**, 29–46 (2005).
37. R. L. Rudnick and D. M. Fountain, "Nature and Composition of the Continental Crust: a Lower Crustal Perspective," Rev. Geophys. **33**, 267–309 (1995).
38. S. S. Sun and W. F. Mc Dunough, "Chemical and Isotopic Systematics of Oceanic Basalts: Implications for Mantle Composition and Processes," in *Magmatism in the Ocean Basins*, ed. by A. D. Saunders, and M. J. Norry, Geol. Soc. London Spec. Publ. **42**, 313–345 (1989).
39. M. Wilson, A. Tankut, and N. Gulec, "Tertiary Volcanism on the Galatia Province, North-West Central Anatolia, Turkey," Lithos, **42**, 105–122 (1997).
40. S. F. Foley and G. E. Wheller, "Paralells in the Origin of the Geochemicat Signatures of Island Arc Volcanics and Continental Potassic Igneous Rocks: The role of Residual Titanates," Chem. Geol. **85**, 1–18. (1990).
41. S. Conticelli and A. Peccerillo, "Petrology and Geochemistry of Potassic and Ultrapotassic Volcanism in Central Italy: Petrogenesis and Inferences on the Evolution of the Mantle Sources," Lithos **28**, 221–240 (1992).
42. Y. Tatsumi, D. Hamilton, and R. W. Nesbitt, "Chemical Characteristics of Fluid Phase Released from a Subducted Lithosphere and Origin of Arc Magmas: Evidence from High Pressure Experiments and Natural

Rocks," J. Volcanol. Geotherm. Res. **29**, 293–309 (1986).

43. A. J. Stoltz, K. P. Jochum, B. Spettel, and A. W. Hoffmann, "Fluid- and Melt-Related Enrichment in the Sub-Arc Mantle: Evidence from Nb/Ta Variations in Island Arc Basalts," Geology **24**, 587–590 (1996).
44. O. Eklund, D. Konopelko, H. Rutanen, et al., "1.8-Ga Svecofennian Post-Collisional Shoshonitic Magmatism in the Fennoscandian Shield," Lithos. **45**, 87–108 (1998).
45. C. Hawkesworth, S. Turner, D. Peate, et al., "Elemental U and Th Variations in Island Arc Rocks: Implications for U-Series Isotopes," Chem. Geol. **139**, 207–211 (1997).
46. O. Elliot, T. Plank, T. Zindler, and W. White, and A. Bourdon, "Element Transport from Slab to Volcanic Front at the Mariana Arc," J. Geophys. Res. **102**, 14991–15019 (1997).
47. D. W. Peate, J. A. Pearce, C. J. Hawkesworth, et al., "Geochemical Variations in Vanuatu Arc Lavas: the Role of Subducted Material and Variable Mantle Wedge Composition," J. Petrol. **38**, 1331–1358 (1997).
48. A. Peccerillo, "Plio-Quaternary Magmatism in Italy," Episodes **26** (3). 222–226. (2003).
49. A. Peccerillo, "Multiple Mantle Metasomatism in Central-Southern Italy: Geochemical Effects, Timing and Geodynamic Implications," Geology **27**, 315–318 (1999).
50. S. F. Foley, "Petrogenetic Characterization of the Source Components of Potassic Magmas: Geochemical and Experimental Constraints," Lithos. **27**, 187–204 (1992).
51. D. A. Jonov, W. I. Griffin, and S. Y. O' Reilly, "Volatile Bearing Minerals and Lithophile Trace Elements in the Upper Mantle," Chem. Geol. **141**, 153–184 (1997).
52. S. Turner, C. Hawkesworth, P. Van Calsteren, et al., "U-Series Isotopes and Destructive Plate Margin Magma Genesis in the Lesser Antilles," Earth Planet. Sci. Lett. **142**, 191–207 (1996).
53. R. L. Romer and H. J. Forster, Breitkreuz C, "Intracontinental Extensional Magmatism with a Subduction Fingerprint: the Late Carboniferous Halle Volcanic Complex (Germany)," Contrib. Mineral. Petrol. **141**, 202–221 (2001).
54. R. W. Maitre, P. Bateman, A. Dudek, et al., "Classification of Igneous Rocks and Glossary of Terms. Recommendations of the International Union of Geological Sciences, Subcommission on the Systematics of Igneous Rocks," (Blackwell, Oxford, 1989).
55. T. N. Jrvine and W. R. A. Baragar, "A Guide to the Chemical Classification of the Common Volcanic Rocks," Can. J. Earth Sci. **8**, 523–548 (1971).
56. A. L. Streckeisen and R. W. Lemaitre, "A Chemical Approximation to the Modal QAPF Classification of the Igneous Rocks," Neues Jahrb. Mineral., Abh. **136**, 169–206 (1979).
57. J. A. Pearce, "Trace Element Characteristics of Lavas from Destructive Plate Boundaries," in *Andesites, Orogenic Andesites and Related Rocks* (Wiley, Chichester, 1982), pp. 525–548 (1982).